Supplementary Information (SI) for Dalton Transactions.
This journal is © The Royal Society of Chemistry 2025

Supplementary information

Impacts of β-Diketonate Terminal Ligands on Slow Magnetic Relaxation and Luminescence Thermometry in Dinuclear Dy^{III} Single-Molecule Magnets

Airton Germano Bispo-Jr,[a,b] Diogo Alves Gálico,[a] Jeffrey S. Ovens,[a] Fernando Aparecido Sigoli,*[b] Muralee Murugesu*[a]

Contents

Supplementary note S1 - Experimental procedure

All reagents and solvents were purchased from AmBeed, Strem Chemicals, Oakwood Chemical, and Thermo Fisher Scientific and used without any further purification. The 2,2'-bipyrimidine (bpm) ligand was prepared as described in the literature.[1]

The precursor $[Dy(hexd)_3(H_2O)_2]$ (molecular weight = 537.92 g mol^{-1}) was prepared by reacting 0.2000 g (1.75 mmol) of the Hhexd ligand with 0.0419 g (1.75 mmol) of LiOH in 10 mL of water. After that, 0.2197 g (0.583 mmol) of $DyCl_3 \cdot 6H_2O$ in 10 mL of water was added to the deprotonated ligand solution and a white precipitate was observed. After two hours of stirring, the white precipitate was filtered, washed several times with water, and vacuum dried for 24 hours. The precursor $[Dy(hpd)_3(H_2O)_2]$ (molecular weight = 580.01 g mol^{-1}) was prepared following the aforementioned procedure, but using 0.5000 g (3.90 mmol) of the Hhpd ligand, 0.0934 g of LiOH (3.90 mmol), and 0.4900 g (1.3 mmol) of $DyCl_3 \cdot 6H_2O$.

For the synthesis of $[Dy_2bpm(hexd)_6]$ (**1**), 0.2000 g (0.37 mmol) of $[Dy(hexd)_3(H_2O)_2]$ was dissolved in 10 mL of methanol. After that, 0.0292 g (0.185 mmol) of bpm dissolved in 10 mL of MeOH was added to the $[Dy(hexd)_3(H_2O)_2]$/methanol solution. The final solution was then refluxed for 4 hours. In the sequence, the solution was cooled down to room temperature and left at 2 °C to slowly evaporate. In two days, colorless blocks of single crystals were observed. $[Dy_2bpm(hpd)_6]$ (**2**) was synthesized by applying the aforementioned procedure and using 0.290 g (0.50 mmol) of $[Dy(hpd)_3(H_2O)_2]$ and 0.0395 g (0.25 mmol) of bpm. A scheme representing the synthesis of complexes **1** and **2** is reported in Figure S1.

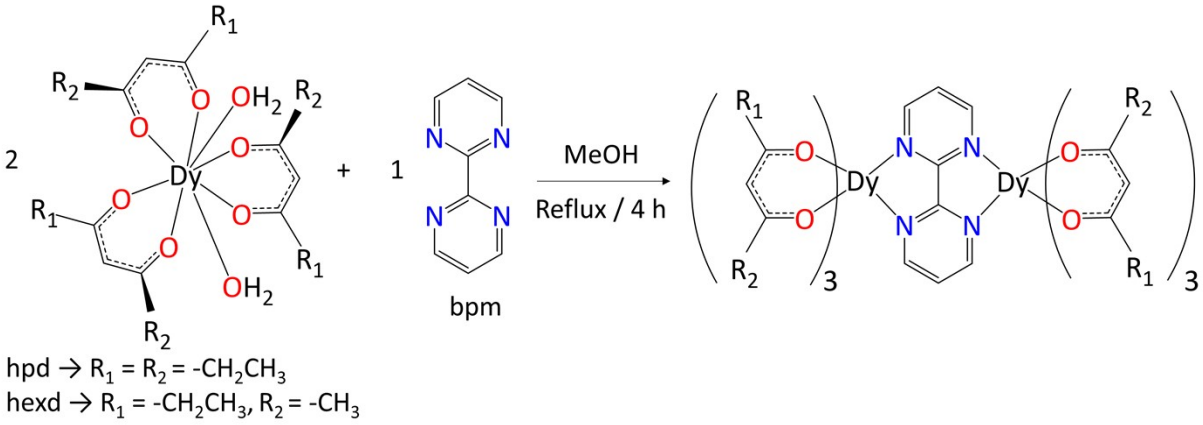

Figure S1. Synthesis of complexes **1** and **2**.

$[Dy_2bpm(hexd)_6]$ (**1**): synthetic yield (50%, molecular weight = 1161.96 g mol^{-1}, 0.1075 g). FTIR (cm^{-1}), Figure S2: 3078 (w), 2966 (w), 2933 (w), 2866 (w), 1587 (s), 1573 (s), 1564 (s), 1512 (s), 1452 (s), 1414 (s), 1398 (s), 1357 (m), 1324 (m), 1256 (w), 1231 (m), 1218 (m), 1177 (m), 1144 (w), 1108 (w), 1066

(m), 1018 (m), 980 (m), 952 (m), 878 (m), 829 (m), 801 (w), 784 (w), 757 (s), 687 (w), 662 (m). Anal. Calcd (%) for **1** (1161.96 g mol^{-1}): C, 45.48; H, 5.20; N, 4.84. Found: C, 45.61; H, 4.85; N, 4.87.

$[Dy_2bpm(hpd)_6]$ (**2**): synthetic yield (55%, molecular weight = 1246.11 g mol^{-1}, 0.1713 g). FTIR (cm^{-1}), Figure S2: 3081 (w), 2969 (w), 2934 (w), 2909 (w), 2873 (w), 1589 (s), 1571 (s), 1566 (s), 1509 (s), 1440 (s), 1422 (s), 1402 (s), 1375 (m), 1366 (m), 1346 (w), 1330 (m), 1304 (m), 1248 (w), 1231 (m), 1216 (m), 1179 (m), 1171 (m), 1105 (w), 1063 (s), 1017 (m), 1003 (m), 980 (m), 950 (m), 878 (m), 852 (m), 833 (m), 808 (w), 784 (w), 757 (s), 687 (w), 662 (m). Anal. Calcd (%) for **2** (1246.11 g mol^{-1}): C, 48.19; H, 5.82; N, 4.51. Found: C, 48.44; H, 5.47; N, 4.54.

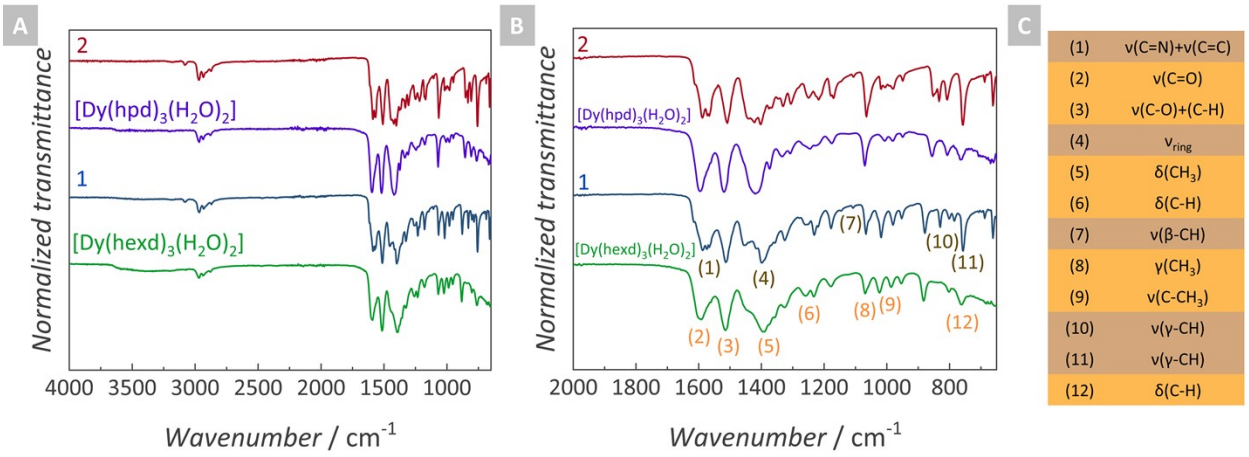

Figure S2. (a) FTIR spectra of **1** and **2** compared to the $[Dy(hpd)_3(H_2O)_2]$ and $[Dy(hexd)_3(H_2O)_2]$ precursors. (b) Magnification of the 2000 – 650 cm^{-1} spectral range. (c) bpm (in brown) and $acac^-$ (in orange) vibrational mode assignments.

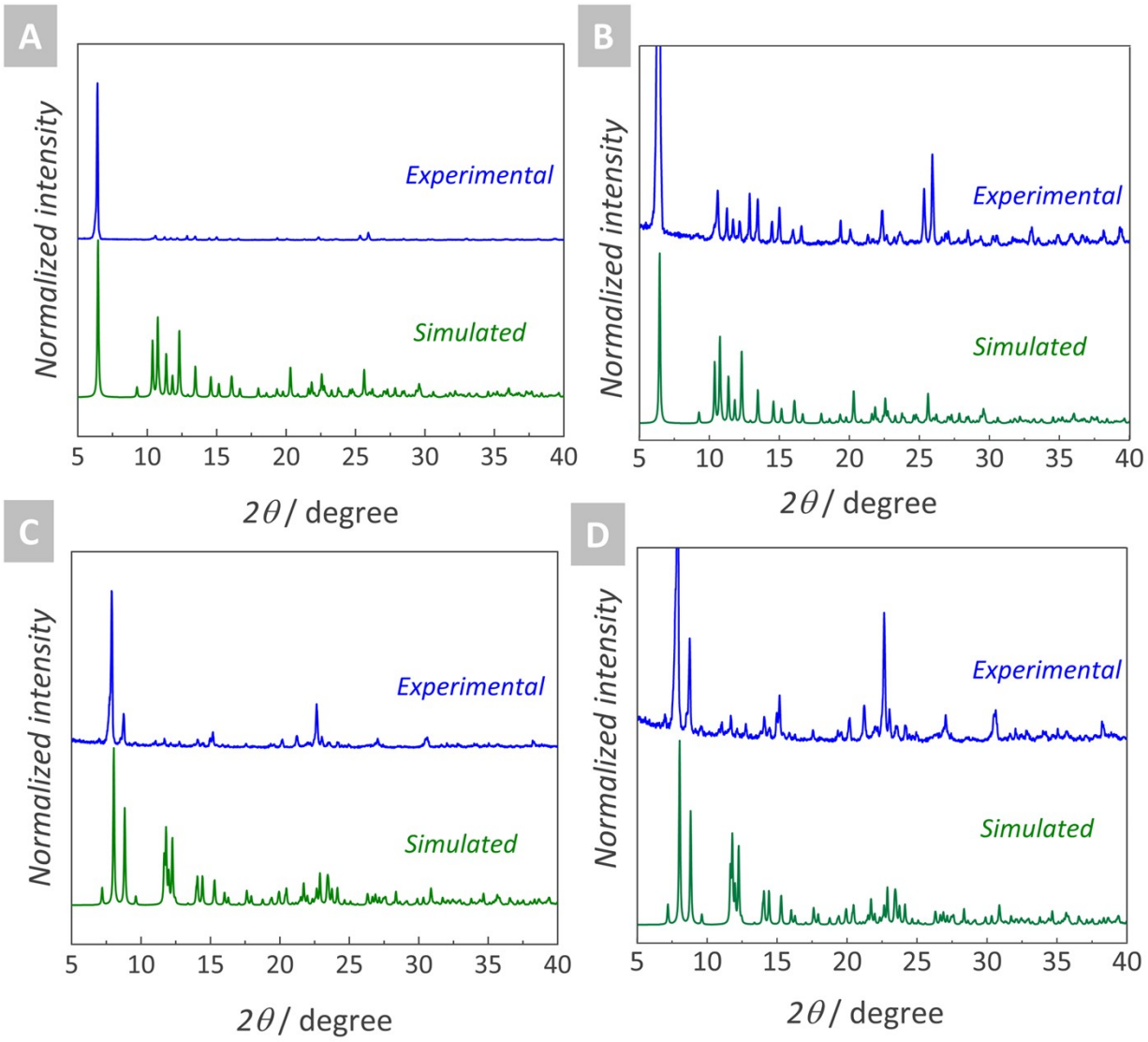

Figure S3. Powder XRD of crashed crystals of (a) **1** and (c) **2** compared to the simulated pattern determined from the SC-XRD. Magnification of the PXRD of (b) **1** and (d) **2**.

Characterization apparatus

Single-crystal X-ray diffraction (SC-XRD): SC-XRD were collected from single crystals of **1** and **2** mounted on MiTeGen MicroMounts using Parabar 10312 oil. Data were collected using Bruker AXS APEX II KAPPA or SMART single crystal diffractometers equipped with sealed tube Mo Kα sources (λ= 0.71073 Å), graphite monochromators, and APEX II CCD detectors. Raw data collection and processing were performed with the APEX II software package from Bruker.[2] Initial unit cell parameters were determined using 36 data frames from selected ω scans. Semi-empirical absorption corrections based on equivalent reflections were applied.[3] Systematic absences in the diffraction dataset and unit cell parameters were

consistent with the assigned space group. The initial structural solutions were determined using ShelXT direct methods,[4] and refined with full-matrix least-squares procedures based on F2 using ShelXL and ShelXle. [5] Hydrogen atoms were placed geometrically and refined using a riding model.

Powder X-ray diffraction (PXRD). PXRD pattern was obtained in a Rigaku Ultima IV diffractometer using Cu K_α filtered radiation (λ = 1.5401 Å) and one diffracted beam monochromator, at 298 K.

Fourier-transform infrared (FTIR). FTIR spectra were recorded in a Thermo Nicolet 6700 FTIR spectrometer using the attenuated total reflection mode and a transmission window from 4000 to 525 cm^{-1}.

Elemental analysis. C, H, N, elementary analysis was measured in a model varioELcube manufactured by Elementar, Germany.

Photoluminescence. All the photoluminescence data were obtained for the crashed crystals using a Quanta Master 8075-21 Spectrofluorometer (Horiba) and a red-extended detector (Hamamatsu R13456 red extended PMT) for the visible spectral region. An ozone-free PowerArc energy 75 W xenon lamp was used as the excitation source. The emission spectra were corrected according to the optical system of the emission monochromator and the photomultiplier response while the excitation spectrum was corrected in real time according to the lamp intensity and the optical system of the excitation monochromator using a silicon diode as a reference.

Temperature-dependent luminescence. Excitation and emission spectra from 9 K to 320 K were measured in the previously mentioned Quanta Master. To control the temperature, a Janis cryostat (CCS-100/204N model) and a Lake Shore temperature controller (model 335) were used.

Magnetism. DC and AC measurements for **1** and **2** were performed using a Quantum Design MPMS3 with 11.6 mg of **1** or 22.1 mg of **2** the crystalline sample, which was restrained with silicon grease and wrapped in a polyethylene membrane. The magnetization data were collected at 100 K to confirm the absence of ferromagnetic impurities. Diamagnetic corrections were applied for the sample holder, and the inherent diamagnetism of the sample was estimated with the use of Pascals constants. In order to extend the probed temperature range, AC susceptibility between 1000 Hz – 10 000 Hz was measured on the same sample using a Quantum D Design Physical Property Measurement System (Dynacool-14T) equipped with a vibrating sample magnetometer (VSM).

Supplementary note S2 - Crystallographic data

Table S1. Crystallographic data of $[Dy_2bpm(hexd)_6]$ (**1**) and $[Dy_2bpm(hpd)_6]$ (**2**).

	1	**2**
CCDC deposition number	2353555	2353556
Empirical formula	$C_{44}H_{60}Dy_2N_4O_{12}$	$C_{50}H_{72}Dy_2N_4O_{12}$
Molecular weight, g mol^{-1}	1161.96	1246.11
Temperature, K	200	200
Wavelength, Å	0.71073	0.71073
Crystal system	Triclinic	Triclinic
Space group	$P\bar{1}$	$P\bar{1}$
a, Å	9.2504(9)	9.3079(6)
b, Å	10.1281(10)	11.8110(8)
c, Å	14.0753(14)	13.0703(9)
α, °	91.315(2)	69.970(1)
β, °	102.365(2)	84.764(2)
γ, °	108.821(2)	80.764(2)
Volume	1213.2	1331.46(16)
No. of formula units/unit cell, Z	1	1
Density (*ρ*), g cm^{-3} calc'd.	1.590	1.554
Absorption coefficient (μ) mm^{-1}	3.117	2.846
F(0 0 0)	580.0	628.0
Crystal size, mm^3	0.14 × 0.09 × 0.02	0.06 × 0.06 × 0.02
Minimum and maximum transmittance	0.667,0.746	0.655,0.745
Theta range, °	1.488 - 28.373	1.660 - 26.405
Index ranges (h k l)	(12 13 18)	(11 14 16)
No. of reflections measured	18083	16998
No. of independent reflections	6067	5442
R(int)	0.049	0.092
Completeness, %	0.999	0.995
Data / restraints / parameters	6067 / 227 / 337	5442 / 118 / 364
R1, wR^2 (I > 2 σ (I))[a]	0.0341, 0.0582	0.0478, 0.0631
R1, wR^2 (all data)	0.0522, 0.0636	0.0881, 0.0733
Goodness of fit on F^2	1.003	1.018
Largest differential peak and hole, e$^-$/Å^3	1.73, −0.62	2.12, −1.51

Table S2. Intramolecular and intermolecular Dy ··· Dy distances (Å) in **1** and **2**.

Distance / Å	**1**	**2**
Intramolecular Dy ··· Dy distance	6.8111(5)	6.8267(5)
Intermolecular Dy ··· Dy distance	7.2849(6)	7.4805(5)

Table S3. Dy – N and Dy – O bond distances (Å) in the first coordination sphere of **1** and **2**.

Bond distances / Å	1	2
Dy – N1	2.5842(26)	2.5858(48)
Dy – N2	2.6164(26)	2.6120(36)
Dy – O1	2.3145(29)	2.3271(33)
Dy – O2	2.2924(29)	2.2998(39)
Dy – O3	2.3281(27)	2.3068(37)
Dy – O4	2.3337(33)	2.2815(36)
Dy – O5	2.3169(22)	2.3106(37)
Dy – O6	2.3085(33)	2.3199(38)
Average Dy – O	2.3157	2.3076

Table S4. Bite angles (°) in **1** and **2**.

Bond Angles / °	1	2
N1 – Dy – N2	62.496(90)	62.216(125)
O1 – Dy – O2	74.000(94)	72.991(131)
O3 – Dy – O4	73.352(93)	75.083(131)
O5 – Dy – O6	73.951(96)	73.444(131)

Table S5. Shape analysis of the Dy^{III} polyhedra in **1** and **2** using SHAPE 2.1. [6] Values in the table are the continuous shape measures (CShM, dimensionless) for each idealized geometry.

Idealized geometry	Short name	Point group	1	2
Square antiprism	SAPR-8	D_{4d}	**0.617**	**0.695**
Biaugmented trigonal prism	BTPR-8	C_{2v}	2.117	2.226
Triangular dodecahedron	TDD-8	D_{2d}	2.473	2.502
Biaugmented trigonal prism J50	JBTPR-8	C_{2v}	2.716	2.845
Snub diphenoid J84	JSD-8	D_{2d}	5.213	5.142
Cube	CU-8	Oh	9.043	8.681
Triakis tetrahedron	TT-8	Td	9.799	9.421
Hexagonal bipyramid	HBPY-8	D_{6h}	15.832	15.285
Johnson gyrobifastigium J26	JGBF-8	D_{2d}	15.817	15.696
Heptagonal pyramid	HPY-8	C_{7v}	21.733	22.013
Elongated trigonal bipyramid	ETBPY-8	D_{3h}	23.625	24.106
Johnson elongated triangular bipyramid J14	JETBPY-8	D_{3h}	27.418	28.094
Octagon	OP-8	D_{8h}	29.401	30.384

Table S6. Skew angle (Ø), magic angle (α), average distances between the coordination atoms in each plane (d_{inn}), interplanar distance (d_{pp}), and dihedral angle (θ) between the upper and lower planes for the Dy^{III} coordination polyhedron compared to an ideal SAP coordination in **1** and **2**.

Parameters	1	2	Ideal SAP
Skew angle (φ) / °	45.008	45.002	45
Compression angle (α) / °	57.360	57.735	54.74
d_{in} / Å	2.836	2.809	$d_{in} = d_{pp}$
d_{pp} / Å	2.557	2.603	
θ / °	1.370	0.699	0

Skew angle (ϕ) = the angle between the diagonals of the two planes, calculated as an average; magic or compression angle (α) = the angle between the S_8 axis and a Dy - ligand direction, calculated as an average. The S_8 axis was considered as the line between the centroids of the upper and lower planes; d_{in} = the average distances between the coordination atoms in each plane defined in the coordination polyhedron; d_{pp} = the interplanar distance, calculated by defining the centroids of the upper and lower planes and then measuring the distances between centroids; θ = the dihedral angle between the upper and lower planes.

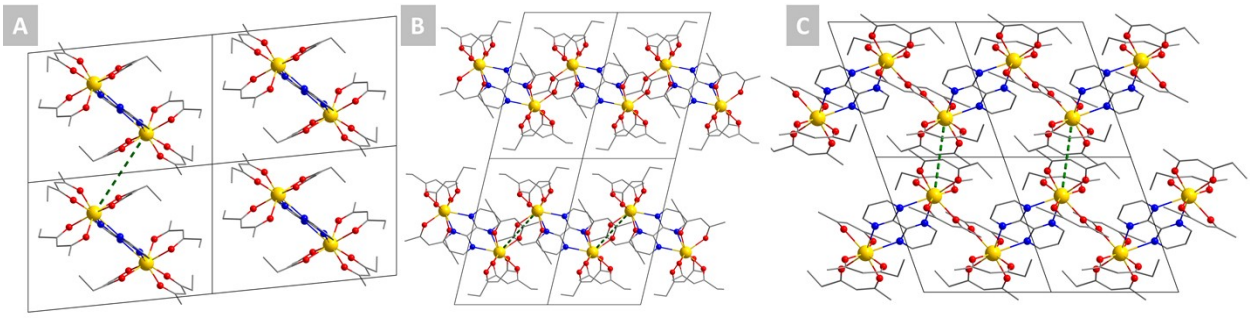

Figure S4. View of the packing arrangement along the crystallographic (a) *a*, (b) *b*, and (c) c-axis in **1**. Green dashed lines represent the shortest Dy · · · Dy intermolecular distance.

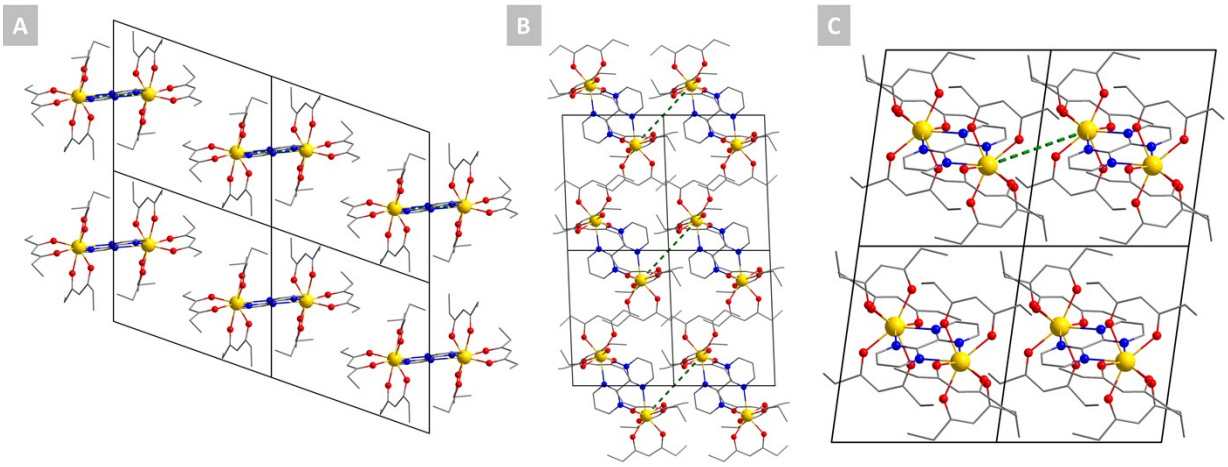

Figure S5. View of the packing arrangement along the crystallographic (a) *a*, (b) *b*, and (c) c-axis in **2**. Green dashed lines represent the shortest Dy · · · Dy intermolecular distance.

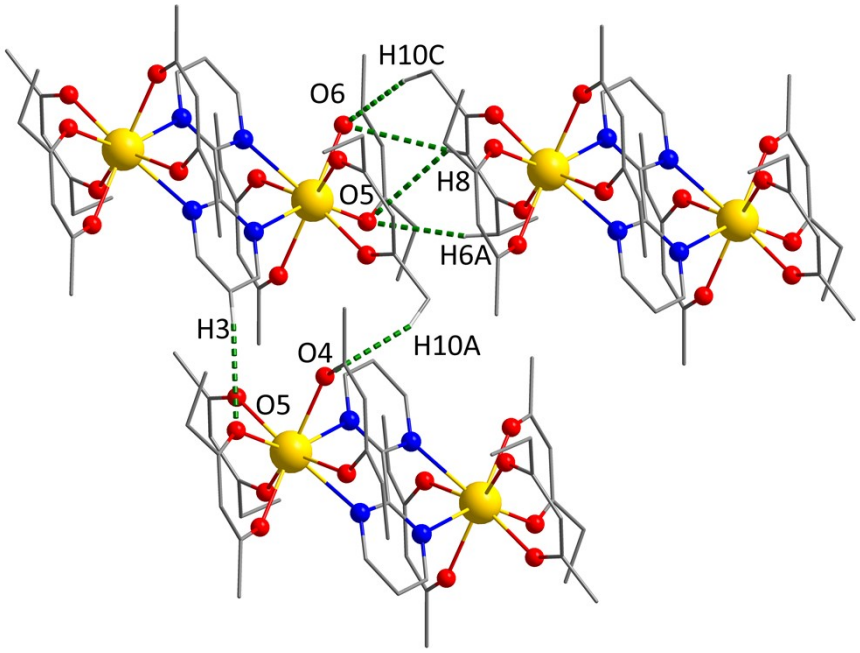

Figure S6. Representation of the intermolecular H-bonds (dashed green lines) in **1**.

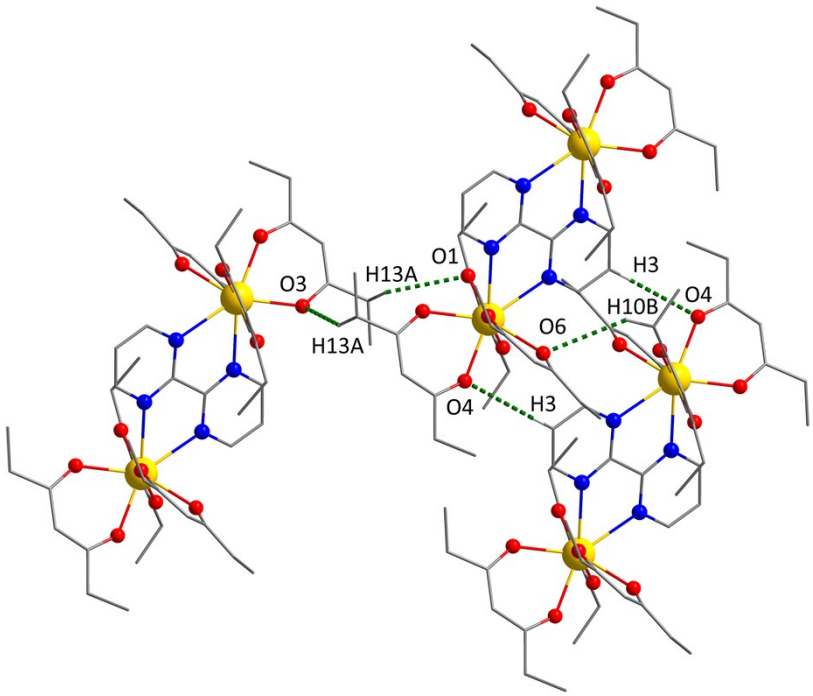

Figure S7. Representation of the intermolecular H-bonds (dashed green lines) in **2**.

Table S7. Intermolecular H-bond distances (Å) in **1** and **2**.

1		**2**	
H3 ··· O5	2.9243(33)	**H3 ··· O4**	2.9405(36)
H10A ··· O4	2.8408(27)	**H10B ··· O6**	3.0577(40)
H10C ··· O6	2.5400(30)	**H13A ··· O1**	2.8630(40)
H8 ··· O6	2.9097(26)	**H13A ··· O3**	2.6950(38)
H8 ··· O5	3.2420(31)		
H6A ··· O5	2.7336(26)		

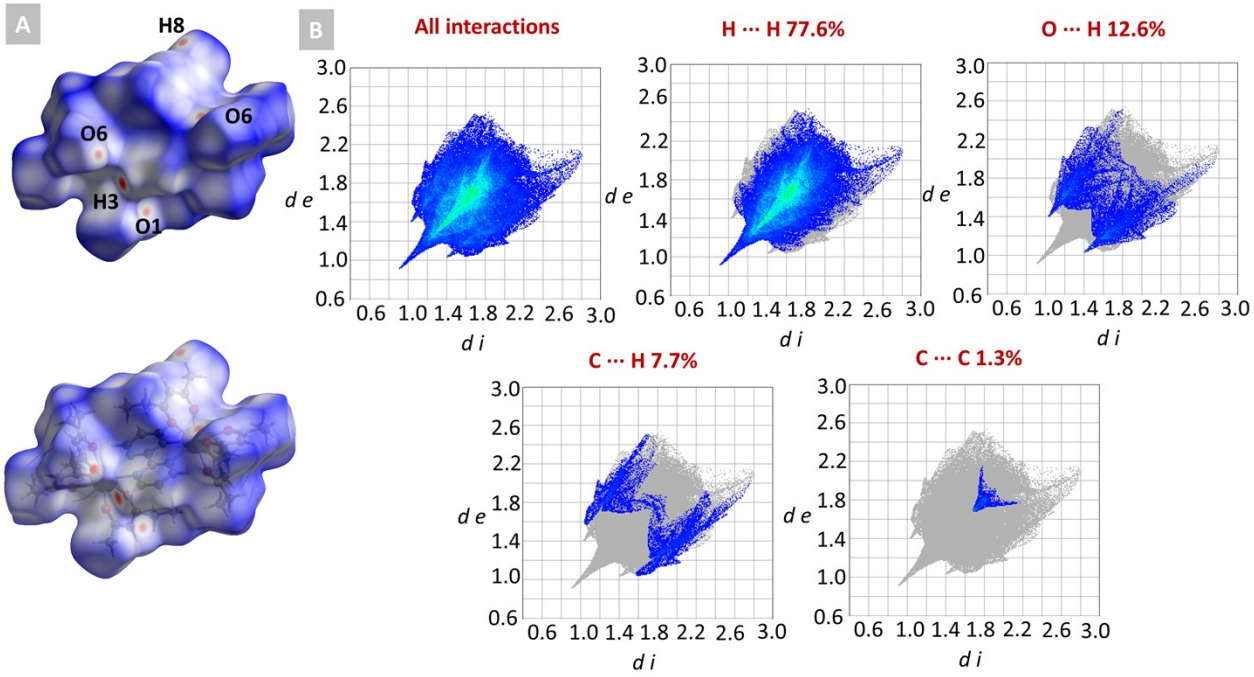

Figure S8. Hirshfeld surface (HS) of **1** mapped over d_{norm} and shape index, *S*. In the d_{norm} HS, a red–blue–white colour scheme was used, whereas red regions represent closer contacts, blue regions represent longer ones, and white regions represent the distance of contacts which is exactly equal to the *vdW* separation. (b) The 2D fingerprint plots of interatomic interactions of **1**, showing the percentages of contacts contributed to the total Hirshfeld surface area of the molecules.

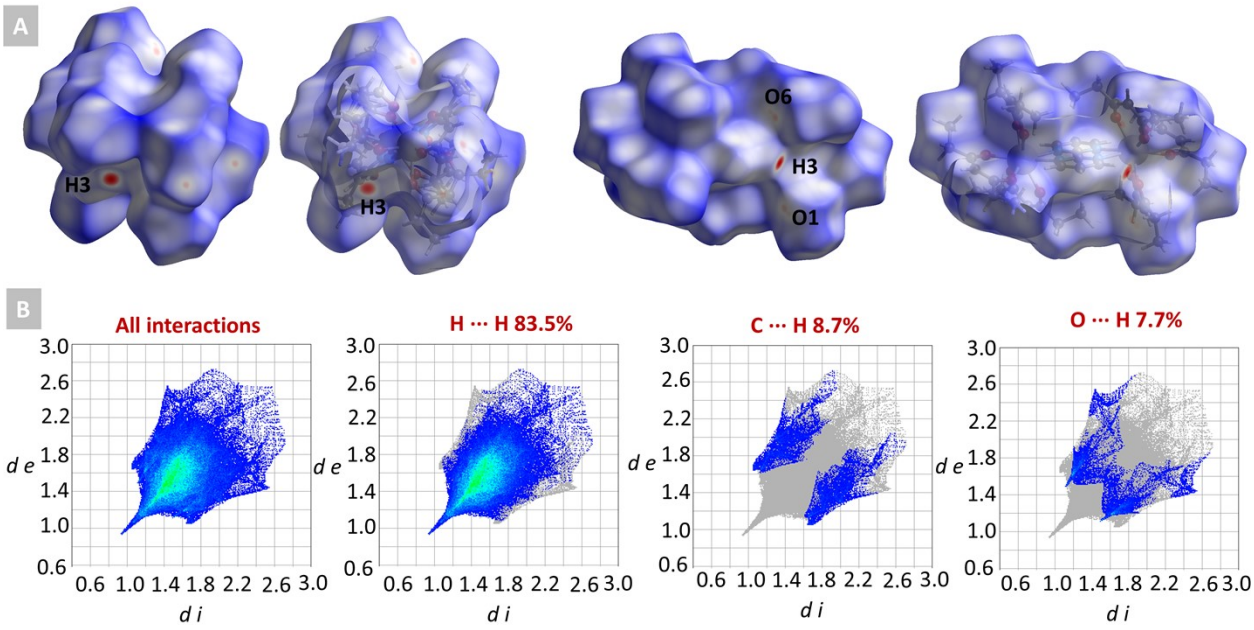

Figure S9. Hirshfeld surface (HS) of **2** mapped over d_{norm} and shape index, *S*. In the d_{norm} HS, a red–blue–white colour scheme was used, whereas red regions represent closer contacts, blue regions represent longer ones, and white regions represent the distance of contacts which is exactly equal to the *vdW* separation. Figure (a) also represents different visualisation angles of the HS. (b) The 2D fingerprint plots of interatomic interactions of **2**, showing the percentages of contacts contributed to the total Hirshfeld surface area of the molecules.

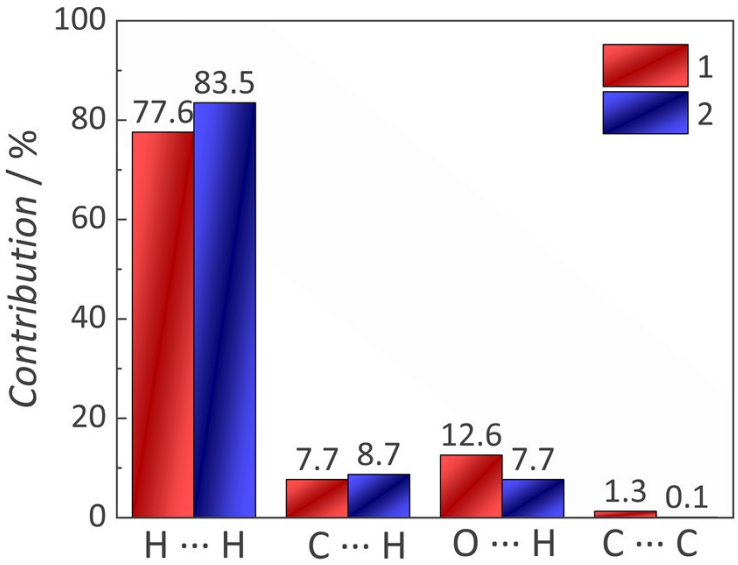

Figure S10. Percentages of contacts that contribute to the total Hirshfeld surface area of the molecules in **1** and **2**.

Supplementary note S3 – Steady state luminescence

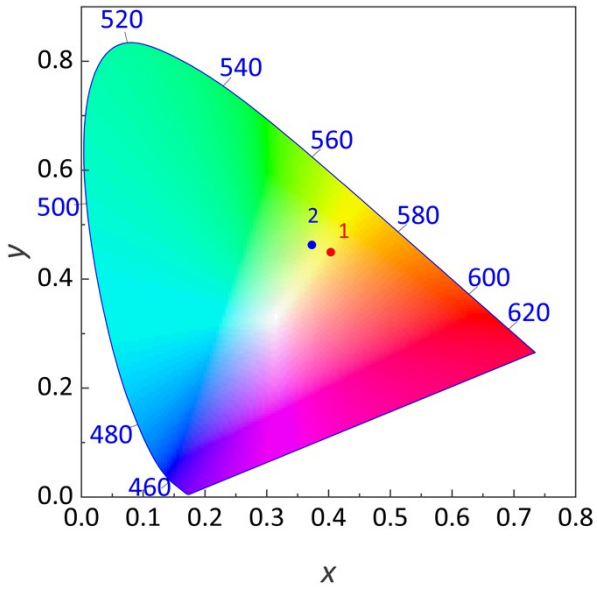

Figure S11. 1931 *Commission internationale de l'éclairage* (CIE) colour coordinate diagram calculated from the emission spectrum of **1** and **2**. The CIE colour coordinates of **1** and **2** are (0.40353;0.44959) and (0.37292; 0.46285), respectively.

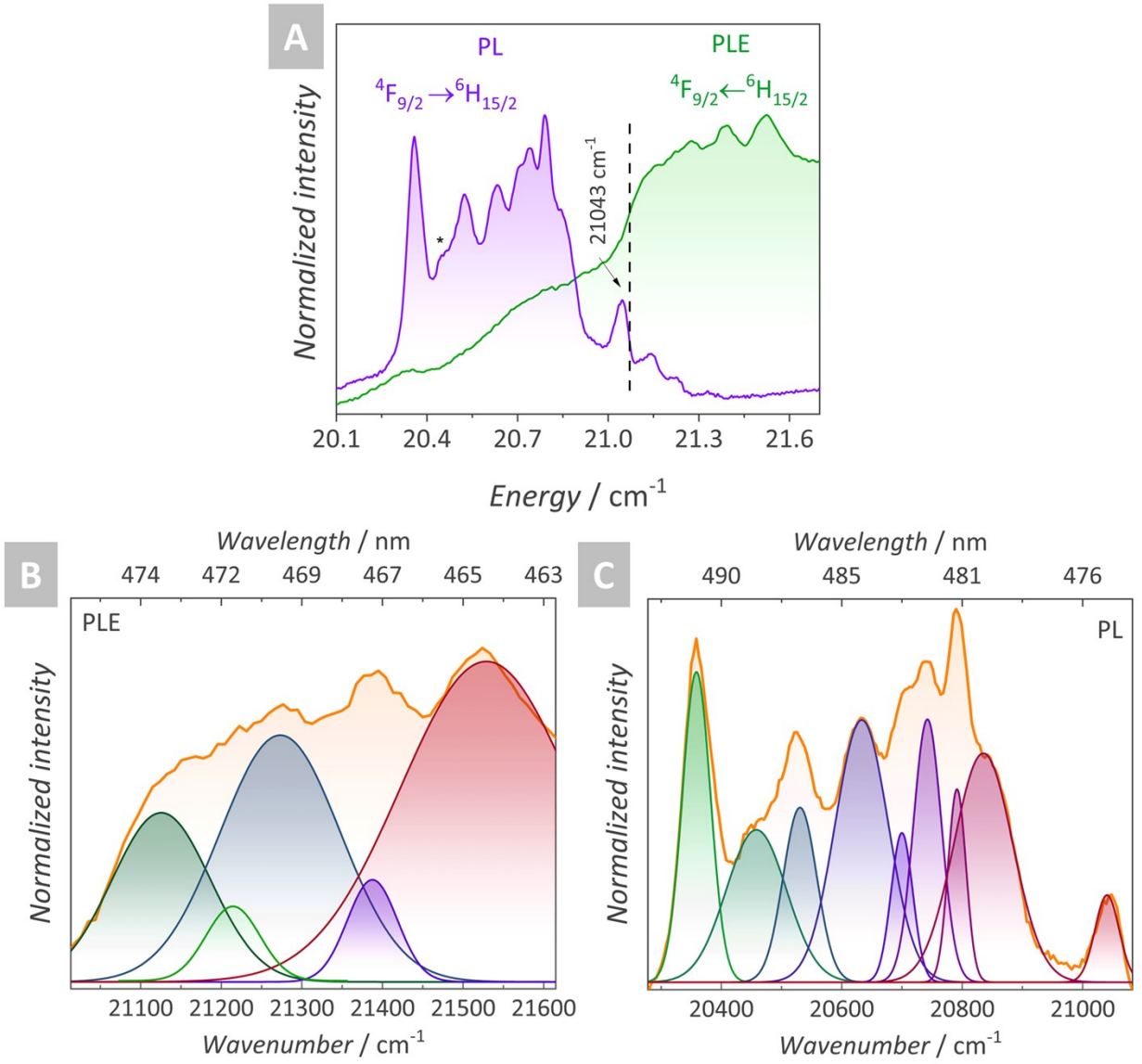

Figure S12. (a) Excitation (PLE, λ_{em} = 575 nm) and emission (PL, λ_{exc} = 305 nm) spectra at 10 K of **1** representing the $^4F_{9/2} \leftarrow {}^6H_{15/2}$ and $^4F_{9/2} \rightarrow {}^6H_{15/2}$ transitions, respectively, used to estimate the energy diagram represented in Figure 2b. Deconvolution of the bands assigned to the (b) $^4F_{9/2} \leftarrow {}^6H_{15/2}$ and (c) $^4F_{9/2} \rightarrow {}^6H_{15/2}$ transitions by applying a gaussian function ($R^2 > 0.99$). The partial energy level diagram was determined as follows: As a consequence of the CF splitting, (J+1/2) M_J (KDs) components are expected for each $^{2S+1}L_J$ level. In the case of the $^6H_{15/2}$ ground level, 8 M_J components are expected in the emission spectrum (assuming that only the first M_J sublevel arising from the $^4F_{9/2}$ emitting level is populated). Yet, additional signals are observed (denoted with* and named as "hot bands"), suggesting that the two lower-energy M_J of the emitting $^4F_{9/2}$ level are populated. Due to the low temperature and according to the Boltzmann distribution, the components arising from the upper energy M_J excited level should render lower intensity emission bands. In light of this guidance, an energetic difference between the M_J sublevels of the ground and emitting levels was obtained, Table S9.

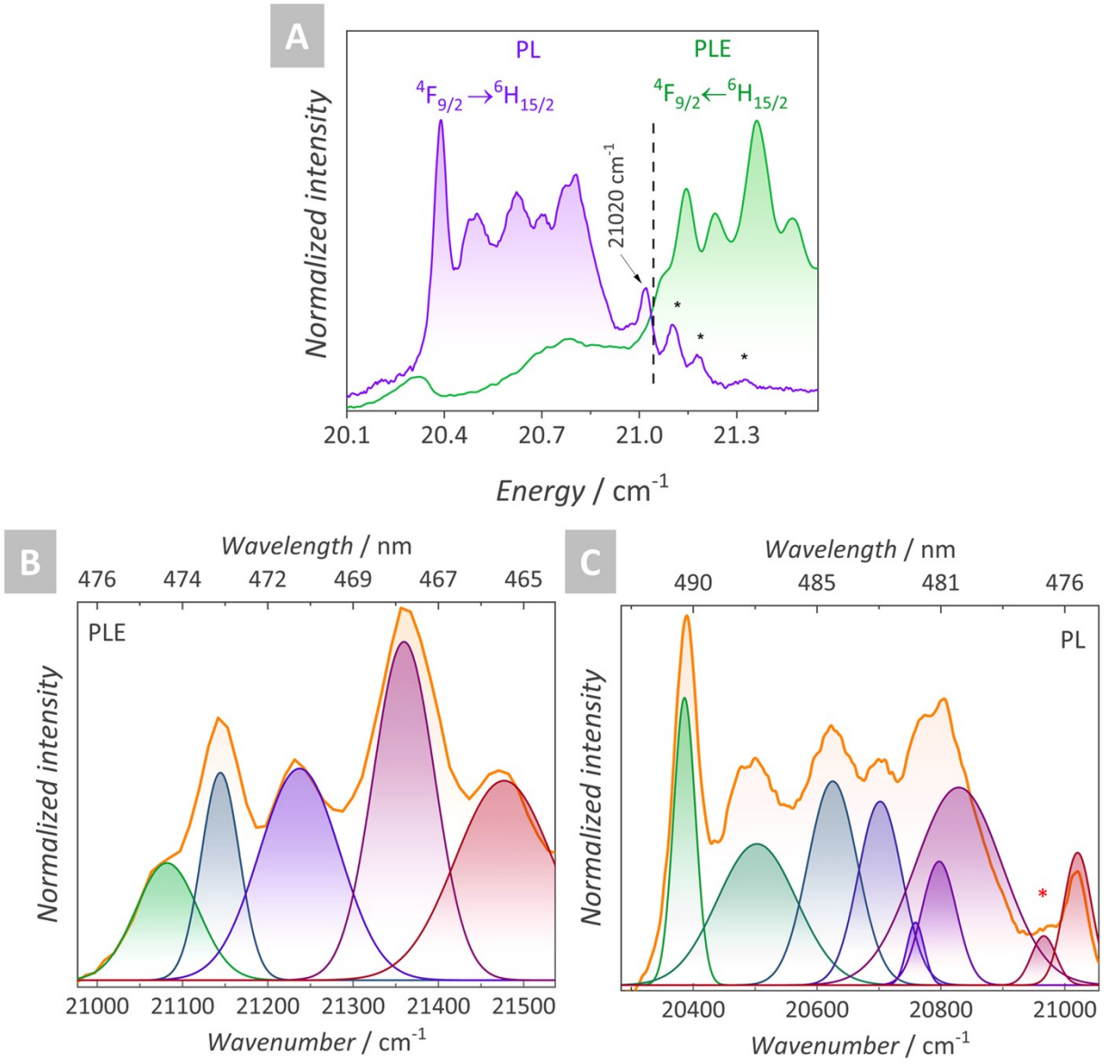

Figure S13. (a) Excitation (PLE, λ_{em} = 575 nm) and emission (PL, λ_{exc} = 305 nm) spectra at 10 K of **2** representing the $^4F_{9/2} \leftarrow {}^6H_{15/2}$ and $^4F_{9/2} \rightarrow {}^6H_{15/2}$ transitions, respectively, used to estimate the energy diagram represented in Figure 2b. Deconvolution of the bands assigned to the (b) $^4F_{9/2} \leftarrow {}^6H_{15/2}$ and (c) $^4F_{9/2} \rightarrow {}^6H_{15/2}$ transitions by applying a gaussian function ($R^2 > 0.99$).

Table S8. Relative energies of the Stark sublevels (M_J or KDs) of the $^6H_{15/2}$ and $^4F_{9/2}$ Dy^{III} levels obtained from the experimental luminescence data of **1** and **2**. ΔE is the energy difference between the KD and the other closest lower energy KD.

	Relative energy / cm^{-1}	ΔE / cm^{-1}	Relative energy / cm^{-1}	ΔE / cm^{-1}
Dy^{III} $^6H_{15/2}$ level	**1**		**2**	
KD1	0	0	0	0
KD2	200 ±2	200	180±4	180
KD3	255±2	55	219±2	39
KD4	304±2	49	251±3	32
KD5	338±3	34	321±4	70
KD6	410±4	72	401±2	80
KD7	523±2	113	525±3	124
KD8	686±2	163	633±3	108
Dy^{III} $^4F_{9/2}$ level				
KD1	21157±5	0	21068±5	0
KD2	21219±3	62	21142±2	74
KD3	21278±5	59	21229±4	87
KD4	21393±2	115	21358±3	129
KD5	21521±12	125	21470±8	112

Supplementary note S4 – Additional magnetic data

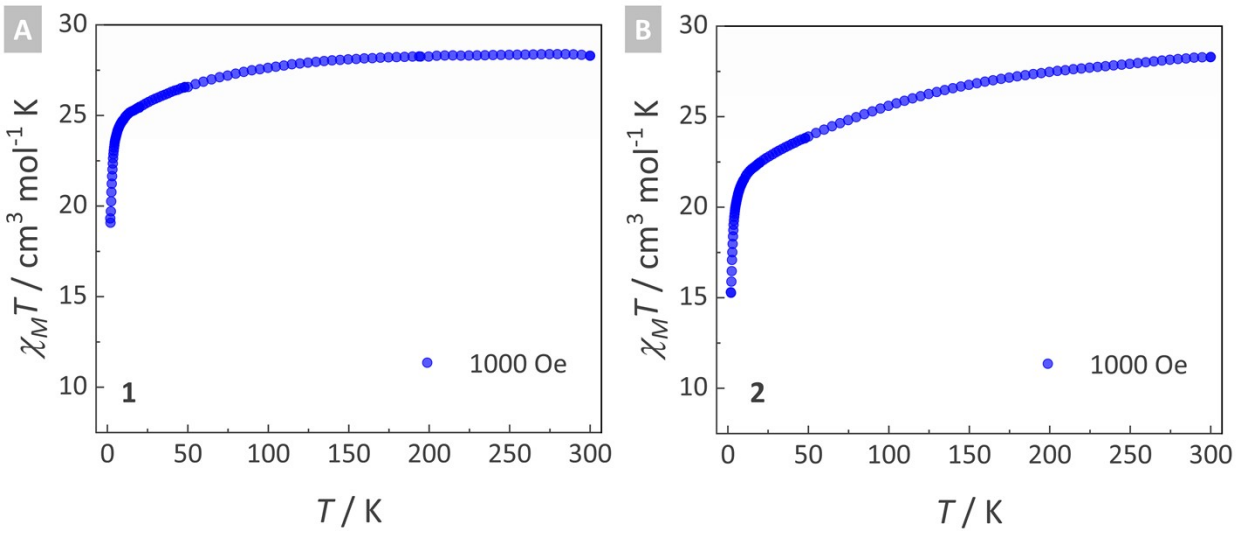

Figure S14. Temperature (T) dependence plot of the magnetic susceptibility ($\chi_M T$) under an applied field of 1000 Oe from 1.8 K to 300 K for (a) **1** and (b) **2**.

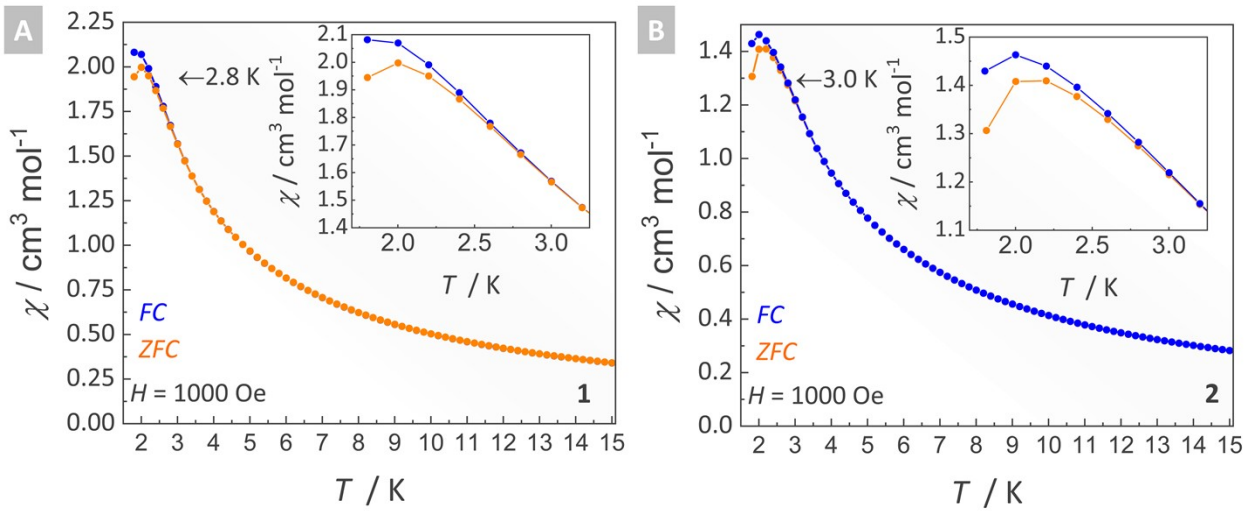

Figure S15. Zero-field-cooled-field-cooled (ZFCFC) measurements (1 K min^{-1}) for (a) **1** and (b) **2**.

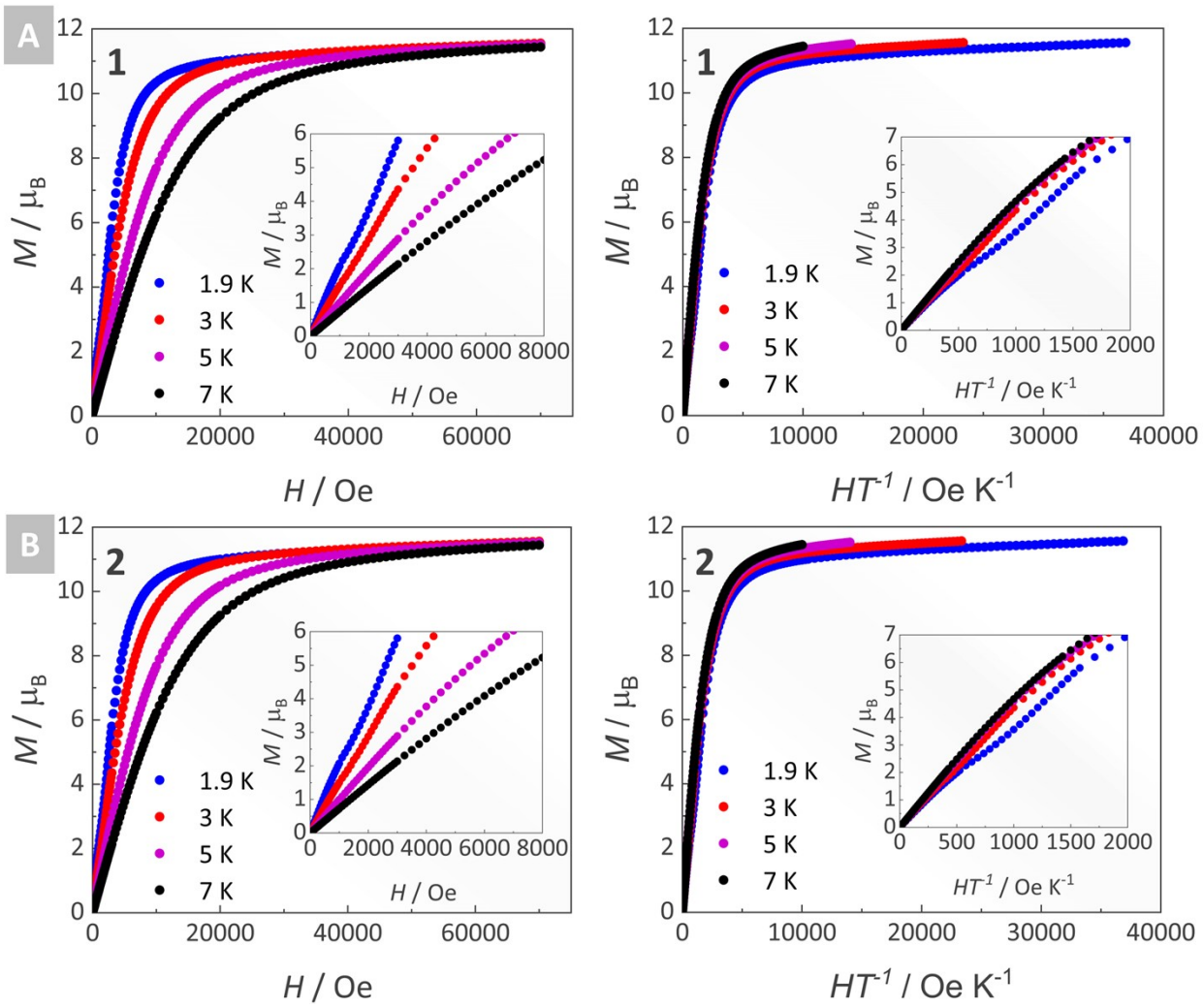

Figure S16. Field (*H*) dependence plot of the (a) magnetization (*M*, left) and the reduced magnetization (HT^{-1}, right) at different temperatures (1.9, 3, 5, or 7 K) for (a) **1** and (b) **2**.

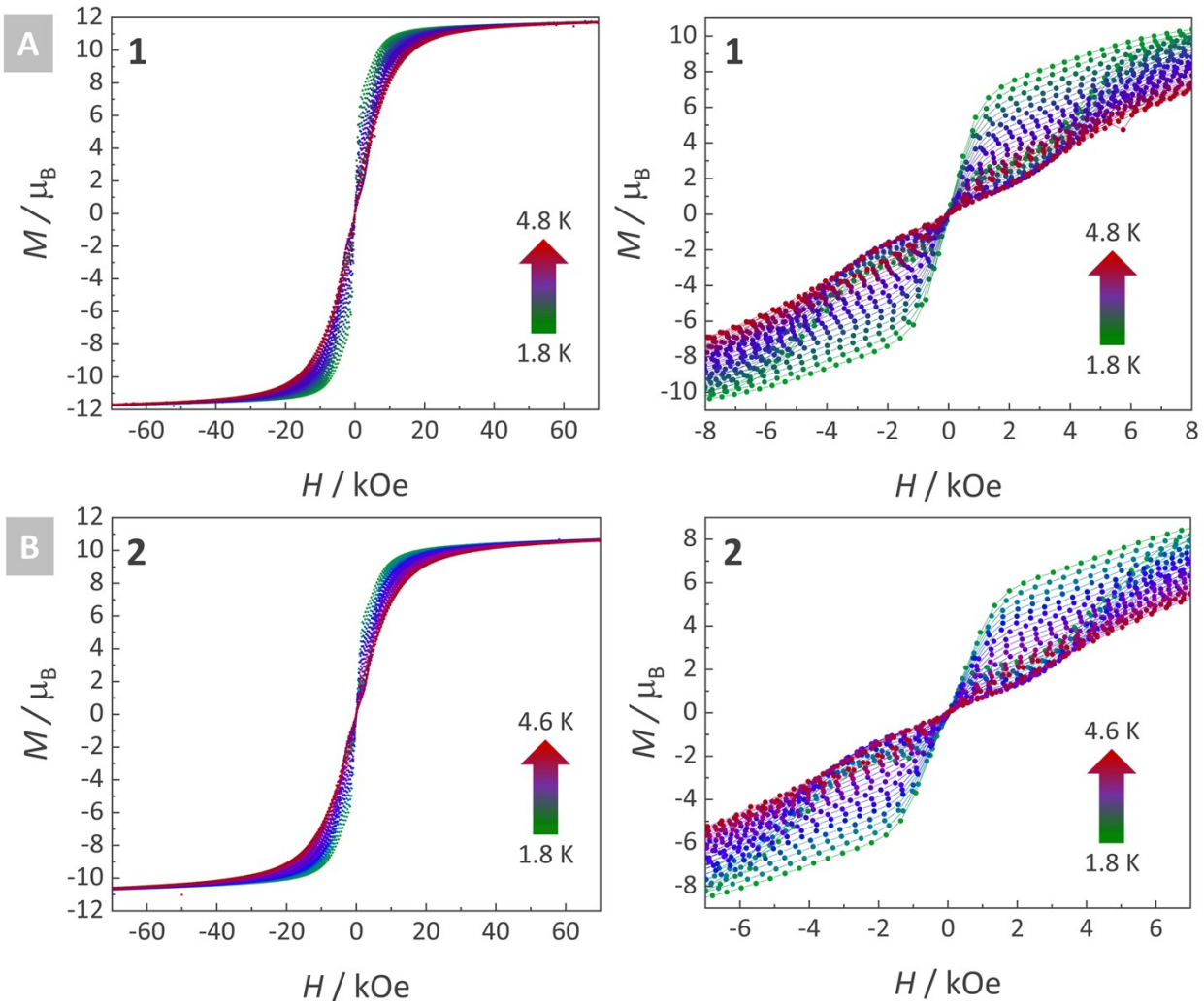

Figure S17. Magnetic hysteresis plot (magnetization *versus* applied field) (sweep rate of 25 Oe s^{-1}) for (a) **1** and (b) **2**.

Alternating current (ac) measurements and data fitting

The χ'' susceptibility curves were fitted using the generalized single (eqn S1) or double (eqn S2) models, where χ_t is the isothermal susceptibility, χ_s the adiabatic susceptibility, ν is the linear frequency, τ is the relaxation time of the magnetization, and the α parameter assumes values between 0 and 1 and gauges the distribution of the relaxation times.[7] The uncertainties of relaxation time parameter were calculated accordingly to D. Reta, N. F. Chilton.[8]

$$\chi'' = \frac{(\chi_t - \chi_s)(2\pi\nu t)^{(1-\alpha)}\cos\left(\frac{\alpha\pi}{2}\right)}{\left[1 + (2(2\pi\nu t)^{(1-\alpha)})\sin\left(\frac{\alpha\pi}{2}\right) + (2\pi\nu t)^{2(1-\alpha)}\right]} \quad (S1)$$

$$\chi'' = \frac{(\chi_t - \chi_s)(2\pi\nu t)^{(1-\alpha)}\cos\left(\frac{\alpha\pi}{2}\right)}{\left[1 + (2(2\pi\nu t)^{(1-\alpha)})\sin\left(\frac{\alpha\pi}{2}\right) + (2\pi\nu t)^{2(1-\alpha)}\right]} + \frac{(\chi_{tg} - \chi_{sg})(2\pi\nu t_g)^{(1-\alpha_g)}\cos\left(\frac{\alpha_g\pi}{2}\right)}{\left[1 + \left(2(2\pi\nu t_g)^{(1-\alpha)}\right)\sin\left(\frac{\alpha_g\pi}{2}\right) + (2\pi\nu t_g)^{2(1-\alpha_g)}\right]} \quad (S2)$$

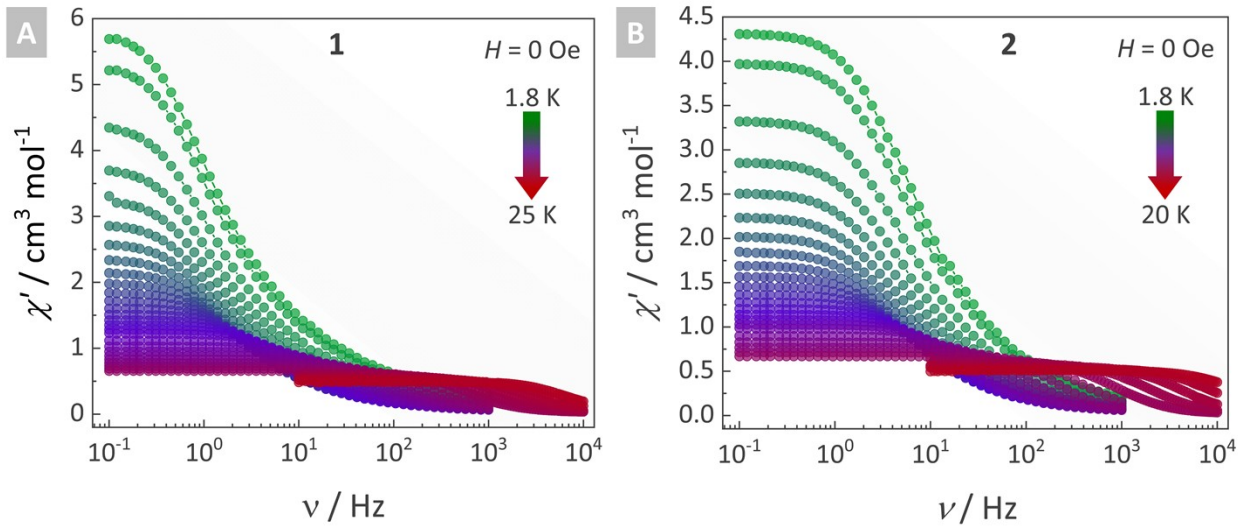

Figure S18. Frequency (ν) dependence of the in-phase (χ') magnetic susceptibility as a function of temperature (T) obtained at zero Oe for (a) **1** and (b) **2**.

Table S9. Best-fit parameters (χ_s, χ_t, α, τ) to the generalized single (7 – 25 K) or double (1.8 – 6.5 K) Debye model for the frequency (ν) dependence of the out-of-phase magnetic susceptibility (χ'') as a function of the temperature (T) for **1**. Data collected at O Oe.

T K	χ_s $cm^3\ mol^{-1}$	χ_t $cm^3\ mol^{-1}$	α	τ s	χ_{s2} $cm^3\ mol^{-1}$	$\chi_{t\,2}$ $cm^3\ mol^{-1}$	α_2	τ_2 s
	LF				*HF*			
1.8	0.08479	3.09118	0.08523	0.16769	0.02039	2.75151	0.43162	0.02048
2	0.89758	3.65913	0.07363	0.16355	0.02039	2.45334	0.41563	0.01906
2.5	0.62478	2.9286	0.07737	0.15372	0.02093	2.01413	0.41585	0.01896
3	0.73513	2.69604	0.07674	0.14726	0.02093	1.72024	0.41396	0.01885
3.5	0.15322	1.88555	0.07187	0.14075	0.02093	1.45457	0.4011	0.01745
4	0.11536	1.67015	0.0752	0.13276	0.0053	1.28009	0.40334	0.01711
4.5	0.01039	1.43625	0.07298	0.12363	0.01155	1.1186	0.39741	0.01572
5	0.07758	1.41259	0.06859	0.11285	0.02092	0.96829	0.38807	0.01424
5.5	0.02093	1.23664	0.06582	0.09967	0.05274	0.91253	0.384	0.01313
6	0.03424	1.19872	0.05763	0.08619	0.01989	0.78379	0.3701	0.01172
6.5	0.06078	1.18342	0.05289	0.07197	0.07162	0.73265	0.35577	0.0098
7	0.0012	1.62152	0.208	0.05159	-	-	-	-
7.5	0.00433	1.68497	0.19212	0.03436	-	-	-	-
8	0.35788	1.78805	0.17738	0.02817	-	-	-	-
8.5	0.42849	1.77753	0.16347	0.02287	-	-	-	-
9	0.48546	1.76433	0.15141	0.01852	-	-	-	-
9.5	0.01139	1.22703	0.14174	0.01502	-	-	-	-
10	0.00765	1.1647	0.13449	0.01223	-	-	-	-
11	0.03794	1.09679	0.12205	0.00822	-	-	-	-
12	0.0383	1.0143	0.11005	0.0056	-	-	-	-
13	0.00528	0.90817	0.09942	0.00388	-	-	-	-
14	0.00401	0.84535	0.09192	0.00274	-	-	-	-
15	0.01192	0.79537	0.08242	0.00194	-	-	-	-
16	0.006	0.73959	0.07558	0.00136	-	-	-	-
17	0.00558	0.69458	0.06636	$9.434\ 10^{-4}$	-	-	-	-
18	0.00112	0.6476	0.05568	$6.425\ 10^{-4}$	-	-	-	-
19	0.00546	0.61153	0.04557	$4.289\ 10^{-4}$	-	-	-	-
20	0.016	0.61737	0.07334	$2.622\ 10^{-4}$	-	-	-	-
21	0.02805	0.604	0.06858	$1.653\ 10^{-4}$	-	-	-	-
22	0.00116	0.54885	0.06208	$1.022\ 10^{-4}$	-	-	-	-
23	0.00173	0.51773	0.05431	$6.256\ 10^{-5}$	-	-	-	-
24	0.00348	0.49274	0.05711	$3.782\ 10^{-5}$	-	-	-	-
25	0.00581	0.46448	0.0385	$2.411\ 10^{-5}$	-	-	-	-

Table S10. Best-fit parameters (χ_s, χ_t, α, τ) to the generalized single (7 – 20 K) or double (1.8 – 6.5 K) Debye model for the frequency (ν) dependence of the out-of-phase magnetic susceptibility (χ'') as a function of the temperature (T) for **2**. Data collected at O Oe.

T K	χ_s $cm^3\ mol^{-1}$	χ_t $cm^3\ mol^{-1}$	α	τ s	χ_{s2} $cm^3\ mol^{-1}$	χ_{t2} $cm^3\ mol^{-1}$	α_2	τ_2 s
	LF				*HF*			
1.8	0.12253	1.93771	0.06386	0.03844	0.00203	2.34863	0.30152	0.00689
2	0.05536	1.67393	0.06091	0.04114	0.02123	2.22467	0.30051	0.00754
2.5	0.03329	1.50674	0.07419	0.04331	0.02191	1.74971	0.30676	0.00768
3	0.01179	1.33952	0.08215	0.04481	0.0209	1.44973	0.31105	0.00778
3.5	0.02202	1.1915	0.08663	0.04579	0.00804	1.26245	0.31422	0.00799
4	0.02039	1.0591	0.08743	0.04726	0.02058	1.1398	0.31262	0.00818
4.5	0.26669	1.24034	0.08303	0.04695	0.02093	0.99325	0.31218	0.00809
5	0.1252	1.03548	0.07903	0.04524	0.02039	0.88198	0.30993	0.00779
5.5	0.02039	0.86659	0.07201	0.0419	0.04109	0.81707	0.30417	0.00718
6	0.01306	0.82441	0.05803	0.03793	0.00265	0.70965	0.29333	0.00676
6.5	0.01092	0.7924	0.04749	0.0325	0.00248	0.62189	0.28428	0.00584
7	0.05082	1.35124	0.20337	0.02024	-	-	-	-
7.5	0.00179	1.21513	0.18041	0.01677	-	-	-	-
8	0.02039	1.17014	0.16606	0.0124	-	-	-	-
8.5	0.02399	1.10857	0.14801	0.01027	-	-	-	-
9	0.04061	1.06694	0.13046	0.00846	-	-	-	-
9.5	0.0023	0.97455	0.11659	0.00687	-	-	-	-
10	0.02309	0.952	0.10436	0.00559	-	-	-	-
11	0.00216	0.85595	0.08587	0.00369	-	-	-	-
12	0.00209	0.78699	0.0738	0.00238	-	-	-	-
13	0.0041	0.73262	0.07192	0.00145	-	-	-	-
14	0.00496	0.68424	0.07043	$8.138\ 10^{-4}$	-	-	-	-
15	0.00666	0.63421	0.06978	$4.202\ 10^{-4}$	-	-	-	-
16	0.00202	0.60895	0.10247	$1.845\ 10^{-4}$	-	-	-	-
17	0.00209	0.57846	0.09427	$8.186\ 10^{-5}$	-	-	-	-
18	0.01692	0.56111	0.07709	$3.739\ 10^{-5}$	-	-	-	-
19	0.00204	0.51303	0.0669	$1.818\ 10^{-5}$	-	-	-	-
20	0.00204	0.50051	0.06096	$8.769\ 10^{-6}$	-	-	-	-

Table S11. Summary of the fitting parameters of the temperature (T) dependence of the relaxation rate of magnetization (τ^{-1}) at 0 Oe and 1800 Oe for **1** and 0 Oe and 1600 Oe for **2**.

		1			**2**		
		0 Oe - LF	**0 Oe - HF**	**1800 Oe**	**0 Oe - LF**	**0 Oe - HF**	**1600 Oe**
Orbach	U_{eff}	290±7 K (201±5 cm^{-1})	-	335±11 K (232±8 cm^{-1})	283±9 K (196±6 cm^{-1})	-	288±6 K (200±4 cm^{-1})
	τ_0 / s	$4.2\pm0.3\ 10^{-10}$	-	$4.3\pm0.1\ 10^{-11}$	$6.7\pm0.7\ 10^{-12}$	-	$4.7\pm0.1\ 10^{-12}$
Raman	c / $s^{-1}\ K^{-n}$	$3.6\pm0.3\ 10^{-5}$	-	$1.6\pm0.1\ 10^{-5}$	$1.3\pm0.3\ 10^{-4}$	-	$2.0\pm0.02\ 10^{-5}$
	n	6.1±0.1	-	6.20±0.05	6.0±0.1	-	6.50±0.05
QTM	τ_{QTM} / s	7.55±0.03	$6.29\pm0.04\ 10^{2}$	-	$2.20\pm0.04\ 10^{1}$	$1.30\pm0.04\ 10^{2}$	-

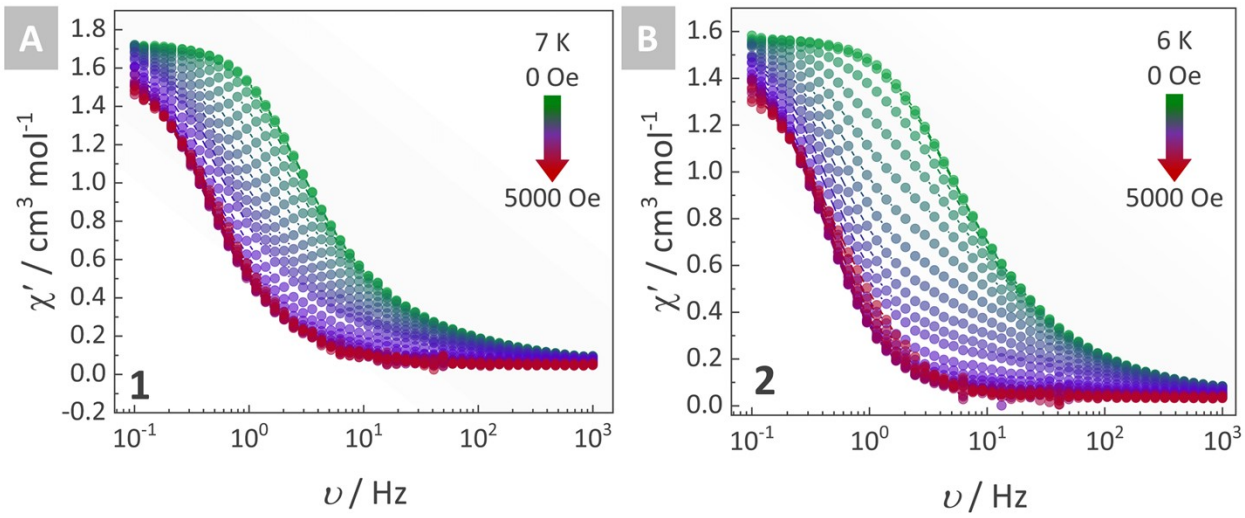

Figure S19. Frequency (υ) dependence of the in-phase (χ') magnetic susceptibility as a function of applied field (H, from 0 Oe to 5000 Oe) (a) at 7 K for **1** and (b) at 6 K for **2**.

Table S12. Best-fit parameters (χ_s, χ_t, α, τ) to the generalized single (1800 – 5000 Oe) or double (0 – 1600 Oe) Debye model for the frequency (υ) dependence of the out-of-phase magnetic susceptibility (χ'') as a function of applied field (H) at 7 K for **1**.

H Oe	χ_s cm³ mol⁻¹	χ_t cm³ mol⁻¹	α	τ^{-1} s⁻¹	χ_s cm³ mol⁻¹	χ_t cm³ mol⁻¹	α	τ s
	HF				*LF*			
0	0.10517	0.68765	0.33929	0.00829	0.00621	1.08301	0.04651	0.05891
100	$5.9867\ 10^{-4}$	0.5768	0.34424	0.00836	0.03384	1.11679	0.05417	0.05958
200	0.0209	0.67034	0.33084	0.00962	$7.39849\ 10^{-5}$	0.99767	0.03859	0.07032
300	$3.53131\ 10^{-6}$	0.67401	0.40991	0.015	0.36949	1.37612	0.1188	0.07782
400	0.00521	0.72191	0.43734	0.02076	0.34345	1.32177	0.14536	0.09891
500	0.00103	0.84401	0.39408	0.02794	0.07015	0.90246	0.10158	0.15559
600	0.01316	0.9353	0.39667	0.03959	0.37458	1.12816	0.05821	0.20554
700	0.02019	0.88719	0.40332	0.04765	0.31442	1.09833	0.04104	0.24197
800	0.02039	0.83069	0.4101	0.05474	0.1074	0.94719	0.03901	0.2684
900	0.01029	0.76165	0.41559	0.0617	0.25468	1.16389	0.04581	0.28766
1000	0.01002	0.72972	0.39983	0.07049	0.30535	1.23292	0.03253	0.31054
1200	0.00146	0.58985	0.41657	0.08496	0.15827	1.23416	0.05715	0.33043
1400	0.09172	0.54477	0.46341	0.12171	0.09555	1.30664	0.07919	0.32627
1600	0.20625	0.54397	0.52203	0.13248	0.00134	1.34299	0.09864	0.33
1800	-	-	-	-	0.00736	1.64029	0.16278	0.3364
2000	-	-	-	-	2.19195	3.81555	0.15392	0.34102
2200	-	-	-	-	0.50801	2.10142	0.14093	0.33735
2400	-	-	-	-	0.83633	2.43999	0.1409	0.33995
2600	-	-	-	-	0.20237	1.79426	0.13837	0.3371
2800	-	-	-	-	0.00743	1.61211	0.14828	0.33505
3000	-	-	-	-	0.00854	1.58371	0.14002	0.32685
3500	-	-	-	-	$7.83611\ 10^{-4}$	1.55561	0.13774	0.31391
4000	-	-	-	-	0.31191	1.82672	0.13068	0.29518
4500	-	-	-	-	0.04219	1.55792	0.14097	0.2756
5000	-	-	-	-	$7.40543\ 10^{-4}$	1.46144	0.12734	0.24793

Table S13. Best-fit parameters (χ_s, χ_t, α, τ) to the generalized single (1600 – 5000 Oe) or double (0 – 1400 Oe) Debye model for the frequency (ν) dependence of the out-of-phase magnetic susceptibility (χ'') as a function of applied field (H) at 6 K for **2**.

H *Oe*	χ_s *cm³ mol⁻¹*	χ_t *cm³ mol⁻¹*	α	τ^{-1} *s⁻¹*	χ_s *cm³ mol⁻¹*	χ_t *cm³ mol⁻¹*	α	τ *s*
	LF				*HF*			
0	0.01306	0.82441	0.05803	0.03793	0.00265	0.70965	0.29333	0.00676
100	0.3293	0.58493	0.00102	0.07051	0.40544	1.65968	0.24425	0.01692
200	0.41592	0.47575	0.00303	0.11379	0.02417	1.50527	0.31737	0.0231
300	0.27133	0.50363	0.00654	0.19771	0.00128	1.31337	0.36025	0.02117
400	0.16853	0.5834	0.00803	0.25833	0.01284	1.14714	0.39096	0.01956
500	0.04475	0.62744	0.01023	0.28657	0.04968	1.01223	0.42521	0.01811
600	0.00137	0.75731	0.01882	0.30574	$6.6154\ 10^{-6}$	0.79365	0.45618	0.01664
700	0.00103	0.9243	0.03365	0.31721	0.02778	0.64268	0.47279	0.0135
800	0.0011	1.06647	0.0519	0.33333	0.1287	0.60469	0.49899	0.01159
900	0.01098	1.19702	0.07145	0.34637	0.0907	0.45781	0.53289	0.00914
1000	0.01605	1.25098	0.07709	0.36181	0.05806	0.42476	0.61922	0.007
1200	0.00456	1.36252	0.08042	0.37	0.10688	0.29693	0.63999	0.00503
1400	0.03406	1.42207	0.08101	0.38228	0.01698	0.26317	0.70625	0.00303
1600	0.00219	1.46001	0.08245	0.38429	-	-	-	-
1800	0.0013	1.4564	0.07636	0.3872	-	-	-	-
2000	0.00137	1.44871	0.06963	0.38616	-	-	-	-
2200	$1.3968\ 10^{-4}$	1.45162	0.07299	0.38378	-	-	-	-
2400	0.01123	1.4567	0.07143	0.3795	-	-	-	-
2600	0.01855	1.45359	0.06674	0.37719	-	-	-	-
2800	0.00209	1.43709	0.07521	0.37141	-	-	-	-
3000	0.00186	1.418	0.06972	0.36215	-	-	-	-
3500	0.06144	1.48351	0.0903	0.34831	-	-	-	-
4000	0.0028	1.38476	0.09104	0.3197	-	-	-	-
4500	$2.1287\ 10^{-4}$	1.40825	0.13331	0.30299	-	-	-	-
5000	0.00329	1.34128	0.13364	0.26367	-	-	-	-

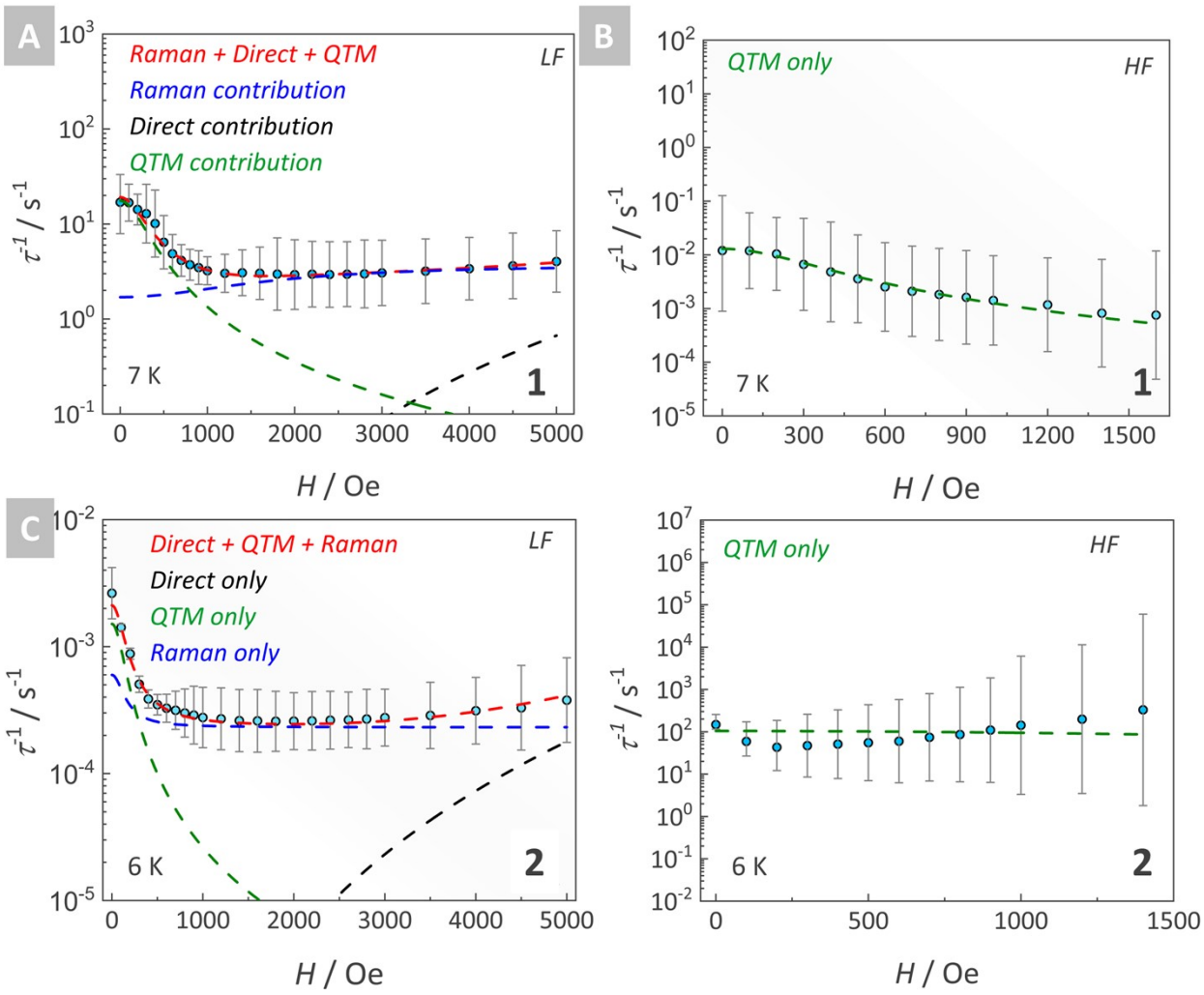

Figure S20. Field (*H*) dependence of the relaxation rate of magnetization (τ^{-1}) at 7 K for **1** and 6 K for **2** considering the (a,c) lower frequency (LF) and (b,d) higher frequency (HF) processes. The solid lines represent the data best fit according to eqn 2, with parameters described in Table S14.

Table S14. Summary of the fitting parameters of the field (*H*) dependence of the relaxation rate of magnetization (τ^{-1}) for **1** and **2**. HF = high frequency, LF = low frequency.

Mechanism	Parameter	1		2	
		LF process	HF process	LF process	HF process
Direct	A / s^{-1} Oe^{-4} K^{-1}	3.6±3.5 10^{-16}	-	4.8±2.1 10^{-16}	-
QTM	$B1$ / s^{-1}	1.73±0.07 10^{1}	1.3±0.08 10^{2}	1.5±0.3 10^{1}	1.0±0.1 10^{2}
	$B2$ / Oe^{-2}	1.2±0.1 10^{-5}	9.3±0.9 10^{-6}	5.7±0.3 10^{-5}	1.0±0.1 10^{-7}
Raman	C / s^{-1} K^{-n}	1.3±0.1 10^{-3}	-	1.3±0.1 10^{-4}	-
	$C1$ / Oe^{-2}	4.9±2.7 10^{-7}	-	2.2±0.6 10^{-5}	-
	$C2$ / Oe^{-2}	2.2±1.6 10^{-6}	-	5.7±1.5 10^{-5}	-
	n	6.4±0.1	-	6.0±0.1	-

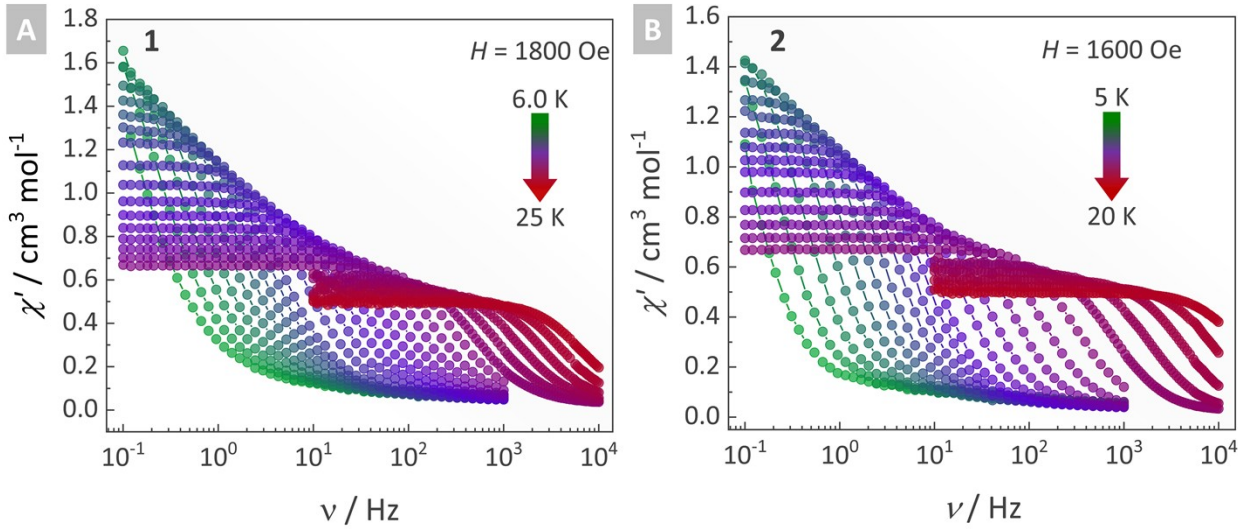

Figure S21. Frequency (ν) dependence of the in-phase (χ') magnetic susceptibility as a function of temperature (T) obtained at (a) 1800 Oe for **1** and (b) 1600 Oe for **2**.

Table S15. Best-fit parameters (χ_s, χ_t, α, τ) to the generalized single Debye model for the frequency (ν) dependence of the out-of-phase magnetic susceptibility (χ'') as a function of the temperature (T) for **1**. Data collected with 1800 Oe.

T / K	χ_s / cm³ mol⁻¹	χ_t / cm³ mol⁻¹	α	τ / s
6.0	0.18088	2.41966	0.24732	1.29222
6.5	0.00887	1.86447	0.19315	0.59321
7.0	0.00452	1.72412	0.17986	0.35423
7.5	0.01096	1.58307	0.15567	0.21483
8.5	0.00209	1.47279	0.1468	0.1393
9	0.02567	1.41366	0.14035	0.09362
9.5	0.00356	1.3106	0.13059	0.06538
10	0.00204	1.24233	0.12718	0.04644
11	0.00254	1.18666	0.12444	0.03395
12	0.01391	1.096	0.12015	0.01935
13	0.02576	1.02185	0.11535	0.01156
14	0.00203	0.9199	0.11255	0.00723
15	0.00293	0.85854	0.10594	0.00466
16	0.00209	0.80388	0.09706	0.00305
17	0.005	0.75282	0.09093	0.00197
18	0.00202	0.70393	0.08085	0.00129
19	0.00192	0.65985	0.07114	$8.2466\ 10^{-4}$
20	0.00251	0.62055	0.05847	$5.1470\ 10^{-4}$
21	0.00209	0.59812	0.09477	$3.0302\ 10^{-4}$
22	0.00334	0.57289	0.09374	$1.8020\ 10^{-4}$
23	0.00243	0.54534	0.08612	$1.0618\ 10^{-4}$
24	0.00209	0.51554	0.07204	$6.3194\ 10^{-5}$
25	0.00209	0.4903	0.06486	$3.7957\ 10^{-5}$

Table S16. Best-fit parameters (χ_s, χ_t, α, τ) to the generalized single Debye model for the frequency (ν) dependence of the out-of-phase magnetic susceptibility (χ'') as a function of the temperature (T) for **2**. Data collected with 1600 Oe.

T / K	χ_s / cm^3 mol^{-1}	χ_t / cm^3 mol^{-1}	α	τ / s
5.0	0.02122	1.85464	0.1353	1.62022
5.5	0.02093	1.62436	0.10907	0.74421
6.0	0.04423	1.53888	0.09223	0.39664
6.5	0.14354	1.52997	0.07736	0.22548
7.0	0.0097	1.30816	0.06759	0.13476
7.5	0.01724	1.22914	0.05566	0.0852
8.5	0.00984	1.15637	0.04868	0.05556
9	0.005	1.09	0.04396	0.03777
9.5	0.00437	1.0328	0.04038	0.02638
10	0.01163	0.99053	0.04292	0.01873
11	0.52302	1.46177	0.04282	0.01349
12	0.00458	0.86322	0.04006	0.00746
13	0.00242	0.79298	0.03986	0.00413
14	0.00327	0.73891	0.04826	0.00224
15	0.00588	0.69133	0.06007	0.00111
16	0.05476	0.69521	0.07322	$5.0631\ 10^{-4}$
17	$7.0886\ 10^{-4}$	0.60669	0.09673	$2.0879\ 10^{-4}$
18	0.00209	0.57327	0.08876	$8.6323\ 10^{-5}$
19	0.01984	0.56023	0.07859	$3.75196\ 10^{-5}$
20	0.0291	0.5345	0.06564	$1.74886\ 10^{-5}$

Supplementary note S5 – Luminescence thermometry

The relative thermal sensitivity of **1** was calculated from eqn S3, where Δ stands for the thermometric parameter and T is the temperature. The temperature uncertainty (δT) was evaluated by means of eqn S4 and eqn S5, where $\delta I/I$ is the relative uncertainty in the integrated area.[9] δI was calculated from the signal-to-noise ratio for each normalized spectrum measured within the 555 – 595 nm spectral range, which was close to 0.015 for all of them. Thus, eqn S5 can be reduced to $\delta I/I$ = 0.010 for all spectra considering the normalized spectra since I_{max} = 1.

$$S_r = \frac{1}{\Delta}\left|\frac{d\Delta}{dT}\right| \quad (S3)$$

$$\delta T = \frac{1}{S_r}\frac{\delta\Delta}{\Delta} \quad (S4)$$

$$\frac{\delta\Delta}{\Delta} = \sqrt{\left(\frac{\delta I_1}{I_1}\right)^2 + \left(\frac{\delta I_2}{I_2}\right)^2} = \sqrt{2}\frac{\delta I}{I} \quad (S5)$$

Table S17. Fitting parameter obtained using a logistic function (eqn S6) to describes the dependence of the thermometric parameter on temperature for **1**.

Parameter	Value
A_1	*9.93*
A_2	*31840*
T_0 / K	*4159*
p	*2.26*

$$\Delta = A_2 + \frac{A_1 - A_2}{1 + \left(\frac{T}{T_0}\right)^p} \quad (S6)$$

Supplementary references

[1] P. F. H. Schwab, F. Fleischer, J. Michl, *J. Org. Chem.*, 2002, **67**, 2, 443.
[2] APEX Software Suite v 2010 Bruker AXS Inc. Madison Wisconsin USA, **2010**.
[3] R. H. Blessing, *Acta Crystallogr. Sect. A* 1995, **A51**, 33.
[4] G. M. Sheldrick, *Acta Crystallogr. A.* 2008 **A*64***, 112.
[5] C. B. Hübschle, G. M. Sheldrick, B. Dittrich, *J. Appl. Crystallogr.* 2011, **44**, 1281.
[6] M. Pinsky, D. Avnir, Continuous Symmetry Measures. 5. The Classical Polyhedra. *Inorg. Chem.*, 1998, **37**, 5575.
[7] S. M. J. Aubin, Z. Sun, L. Pardi, J. Krzystek, K. Folting, L.-C. Brunel, A. L. Rheingold, G. Christou, D. N. Hendrickson, *Inorg. Chem.*, 1999, **38**, 5329.
[8] D. Reta, N. F. Chilton, *Phys. Chem. Chem. Phys.*, 2019, **21**, 23567.
[9] Brites, C. D. S.; Millán, A.; Carlos, L. D. Lanthanides in Luminescent Thermometry. In: Handbook on the Physics and Chemistry of Rare Earths; Elsevier, 2016; pp 339-427.